Fabrication, and direct current and cryogenic analysis of SF6-treated AlGaN/GaN Schottky barrier diodes

Quentin Fornasiero, Nicolas Defrance, Sylvie Lepilliet, Vanessa Avramovic, Yvon Cordier, Eric Frayssinet, Marie Lesecq, Nadir Idir, Jean-Claude de Jaeger

Fabrication, and DC and cryogenic analysis of SF_6-treated AlGaN/GaN Schottky barrier diodes

Quentin Fornasiero[1a], Nicolas Defrance[1], Sylvie Lepilliet[1], Vanessa Avramovic[1], Yvon Cordier[3], Eric Frayssinet[3], Marie Lesecq[1], Nadir Idir[2], Jean-Claude De Jaeger[1]

[1] Univ. Lille, CNRS, Centrale Lille, Univ. Polytechnique Hauts-de-France, UMR 8520 – IEMN – Institut d'Electronique de Microélectronique et de Nanotechnologie, F-59000, Lille, France
[2] Univ. Lille, Arts et Metiers Institute of Technology, Centrale Lille, Junia, ULR 2697-L2EP, F-59000 Lille, France
[3] Université Côte d'Azur, CNRS, CRHEA, rue Bernard Grégory, 06560 Valbonne, France

[a)] Electronic mail: quentin.fornasiero@iemn.fr

Schottky contacts on fluorine implanted AlGaN/GaN heterostructure with ideality factor close to unity and low on-voltage threshold are presented in this paper. A SF_6 plasma anode pre-treatment followed by a specific low-temperature annealing is also compared to a non-annealed sample. In addition, physical-model parameters are extracted by means of cryogenic temperature measurements to understand the conduction mechanisms involved in annealed diodes, showing better DC performances than their non-annealed counterparts. Furthermore, the annealing induces a decrease of the ideality factor, which sets the field-enhanced thermionic emission as the main conduction mechanism, and reduces the tunneling reverse current leakage. This effect is attributed to the recovering of the plasma-induced damages.

I. INTRODUCTION

GaN-based devices are highly suitable for power electronics thanks to their high conductivity and electric field strength that enable low losses and high voltages[1–3] applications. In power converters, the improvement of the on-resistance R_{on} permits higher efficiency[4] and thus increased integrability[5]. For this purpose, Ni/AlGaN Schottky contacts are used as Schottky rectifier diodes or field effect channel control electrode. Such contacts are very suitable in the case of the Lateral Field-Effect Rectifier (LFER) anode because it contributes actively to the channel state switching and also to the overall current driven in the device[6,7].

In this paper, Schottky-diode fabrication processes with Fluorine Plasma Treatment (FPT) on the anode surface are described. FPT is a common GaN device-processing step providing a normally-off operation. It has been already observed that the FPT improves drastically both the forward and reverse characteristics of the Schottky contact on AlGaN compared to an untreated one[8,9]. However, dry fluorinated treatments mainly induce surface damages that introduce undesirable states in the AlGaN layer, and endure thermal instability[10,11], especially following the Schottky anode rapid thermal annealing (RTA). Hence, in this study a specific low temperature annealing (LTA) subsequent to the FPT is experimented for the first time to prevent DC performances degradation. Thus, low turn-on voltage and on-resistance in the forward conduction mode[12–14], and low reverse current leakages[15,16], are obtained on a LTA-based process sample. The measurements revealed a reduction of the ideality factor close to unity on the annealed contacts. To understand the physical mechanisms permitting these results, cryogenic measurements were carried out showing a good fit with the thermionic emission model, while the non-annealed contacts suffer from more tunneling conduction. This effect is produced by the recovering of the plasma induced damages[17–19].

II. DEVICES FABRICATION PROCESS

AlGaN / GaN heterostructures are grown on high-resistive Silicon (111) substrate by Metalorganic Chemical Vapor Deposition (MOCVD). The structure consists of a low-temperature 20 nm thick and a high temperature 200 nm thick AlN nucleation layers, followed by a 350 nm thick C-doped GaN buffer, a 1.5 nm AlN spacer, a 15 nm $Al_{0.3}Ga_{0.7}N$ barrier layer and finally a 5 nm thick SiN cap layer.

Two wafer samples – A and B – are mechanically cleaved from the same epitaxy and are simultaneously processed. Devices fabrication starts with Ti/Al/Ni/Au ohmic contacts evaporation with thicknesses of 12/200/40/100 nm, respectively, followed by a RTA at 850°C for 30 seconds in N_2 atmosphere. In order to electrically isolate devices, a nitrogen ionic implantation is performed to deeply destroy the crystal lattice and cancel the two dimensional electron gas (2DEG)[20]. The ions diffusion is estimated to be approximately 400 nm depth, using TRIM calculations. Then, a 200-nm SiN layer is deposited as passivation layer using a SiH_4 / NH_3 gas mix by plasma enhanced chemical vapor deposition (PECVD) method, at a temperature of 340°C, and at last, samples are annealed during 20 minutes at 400°C in N_2 atmosphere. CHF_3 / CF_4 reactive ion etching (RIE) removes PECVD-SiN passivation and MOCVD-SiN cap layers[21], to release ohmic contacts and AlGaN surface before anode pretreatment and deposition. The key step relies on a SF_6-based hybrid reactive ion etching / inductively coupled plasma (RIE/ICP) treatment as FPT ,set on a 30sccm flow and a pressure of 50mT, at room temperature during 10 minutes. The RIE RF power and the ICP power are 80W and 40W, respectively, and the self-bias voltage is 28 V. This value is relatively low as compared to standard measured voltages regarding AlGaN fluorinated plasma treatment which are typically around 100

V[22,23], but it ensures low damages on the surface[24,25]. LTA is experimented on the sample A, consisting of a first plateau at 250°C and a second at 350°C, each one for 180 minutes, with a slope of 10°C/min, under N_2 atmosphere. No annealing is performed on the sample B counterpart. Subsequently, a Ni/Au Schottky contact deposition is performed with thicknesses of 40 nm and 300 nm, preceded by a smooth Ar^+ beam to clean the AlGaN surface. Then, the contacts are annealed at 400°C for 20 minutes under nitrogen atmosphere. Figure 1a summarizes successive steps of the process flow.

The devices under test, shown in Figure 1b, consist in a dual contact, with anode and cathode surfaces of 100*32 µm², 5 µm apart. Finally, the ohmic contact resistances R_c, obtained by transmission line method, are 0.41 Ω.mm on sample A and 0.68 Ω.mm on sample B, well located in the current state-of-the-art [26–28]. The channel square resistances $R_□$, measured by Hall effect, are 406 Ω/□ and 388 Ω/□, respectively.

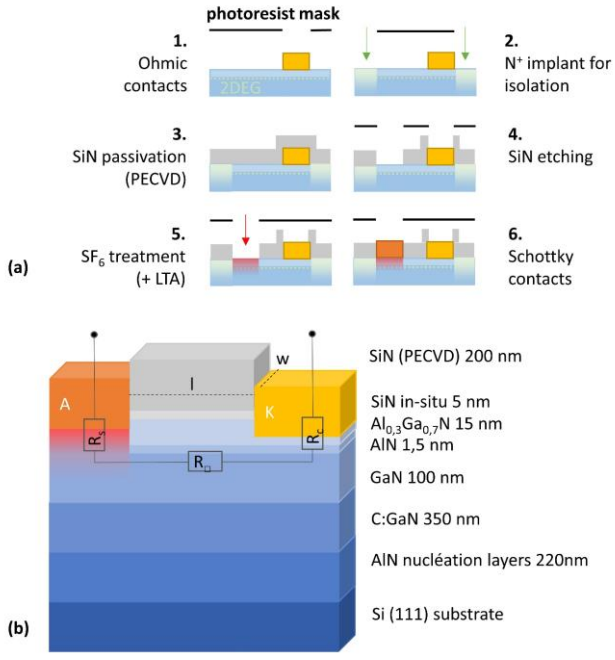

FIGURE 1: Representation of the fabrication process flow (a) and transverse view of epitaxy and device structure (b).

III. RESULTS AND DISCUSSION

A. MEASUREMENTS AT ROOM TEMPERATURE

Five devices of each type are measured with a good repeatability. *Figure 2* shows the static current characteristic of two selected diodes as a function of the forward and reverse voltages. The sample A displays the best performances with a V_{on} (at 1mA/mm) and a total R_{on} (at maximum I-V slope) about 0.54V and 3.7 Ω.mm, respectively. The sample B exhibits the same V_{on} but a R_{on} of 5.2 Ω.mm, which is approximately the on-resistance value found by Chiu et al.[29] for similar GaN Schottky devices with fluorine treatment. Process optimization clearly enables better Schottky diodes performance, but the given R_{on} feature includes the contribution of all partial resistances: R_c, $R_{\square}$, and the Schottky contact resistance R_S. Excluding the cathode contact and channel resistances, the effective Schottky contact resistance, R_S, value is 1.26 Ω.mm and 2.58 Ω.mm on samples A and B, respectively. They are extracted using the following equation:

$$R_S = R_{on} - R_{\square} \cdot \frac{l}{w} - \frac{R_c}{w}, \qquad (1)$$

Where $R_{\square}$ is the channel square resistance, l is the anode-cathode length, R_c is the ohmic contact resistance and w the diode width. The reverse current leakage at -50V are 32 µA/mm and 130 µA/mm on devices A and B, respectively. It is observed that LTA permits reducing of R_S and I_R. The reduction of R_S using the LTA is related to the recovering of the damages induced by fluorine plasma on the crystal structure. Thus, the higher R_{on} on samples B can be attributed to unrecovered damages.

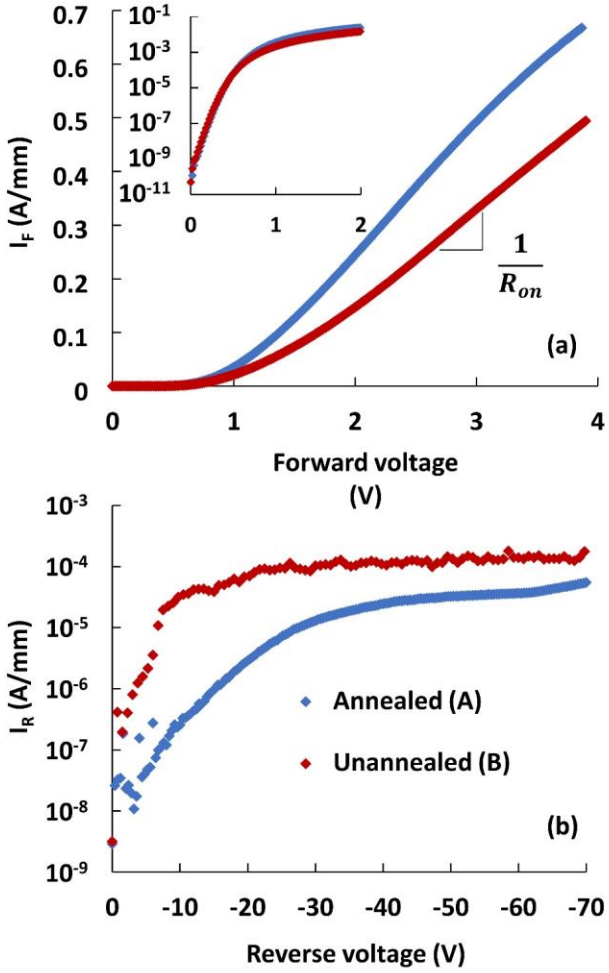

FIGURE 2. Forward (a) and reverse (b) current-voltage characteristic of Schottky diodes.

B. I(V)-TEMPERATURE MEASUREMENTS

For an ideal Schottky contact, the reverse saturation current I_S and the barrier height ϕ_b variations are opposite from each other according to the Schottky-Mott thermionic emission (TE) model, described in equation (2). The higher the barrier is, the lower the saturation current. On the previous devices, the decrease of the reverse current on the post-annealed samples is observed, while V_{on} keeps the same value. It is inconsistent, compared to a pure thermionic emission model.

$$I_S = AA^*T^2\exp\left(-\frac{\phi_b}{kT}\right) \qquad (2)$$

A, A^*, k, T and ϕ_b are the contact surface, the Richardson constant, the measure temperature, the Boltzmann constant and the Schottky barrier height, respectively.

In order to understand the conduction mechanisms through the Schottky contacts, cryogenic temperature measurements are led from 77 K to 300 K in low vacuum ambient of 10^{-6} mbar to avoid the freezing of the air moisture. The tested devices anode length is 3 µm to limit the equivalent parallel resistance. Results of the measurements are plotted in *Figure 3*. Two methods of analysis, based on different representations of a Schottky contact, are studied and compared to explain the different behavior between the samples A and B.

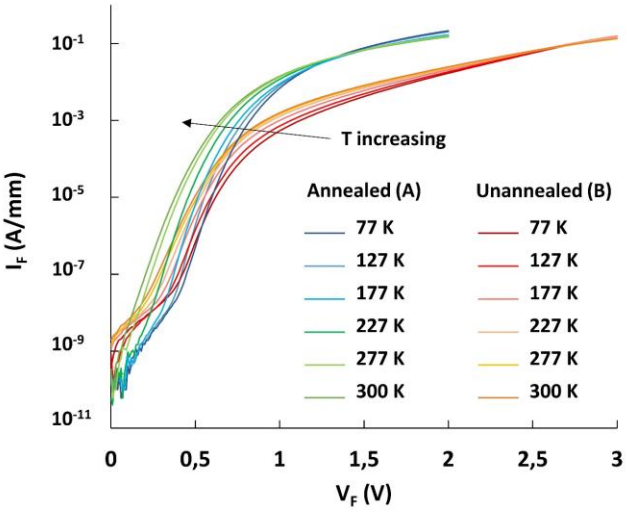

FIGURE 3. Forward current as a function of voltage, plotted at temperatures from 77 K to 300 K.

The first studied model was introduced by Werner and Güttler[30], taking into account barrier height fluctuations along the contact surface. Indeed, the contact inhomogeneity causes local variations of the barrier height, inducing some leakage paths at lower energy

levels. The barrier is represented by its average height $<\phi_b>$ and the standard deviation σ. The origin of these inhomogeneities lay on the defects in material such as dislocations of the AlGaN layer. Thus, $<\phi_b>$ and σ are extracted from the apparent ϕ_b as a function of temperature (*Figure 4*), following the equation:

$$\phi_b(T) = <\phi_b> - \frac{q\sigma^2}{2kT}, \qquad (3)$$

For sample A and B an average barrier of 0.93 eV and 1.01 eV with a standard deviation of 0.12 eV and 0.13 eV respectively, are calculated. This is consistent with other results obtained by the same way. Shin et al[31] and Karboyan et al.[32] demonstrated similar barrier height of 0.98 eV and 1.07 eV, respectively, for Ni/AlGaN contact. Kim et al.[33] found a much higher 1.55 eV barrier height with a deviation of 0.19 eV, using a fluorinated plasma anode-pretreatment on Pt/AlGaN Schottky contact, and Garg et al.[34] showed a 1.79 eV-barrier height using a Cu/AlGaN contact. However, these close values between both samples are not significant when compared to the deviation, and does not explain the different reverse characteristics. Thus, the improvement of the reverse behavior does not

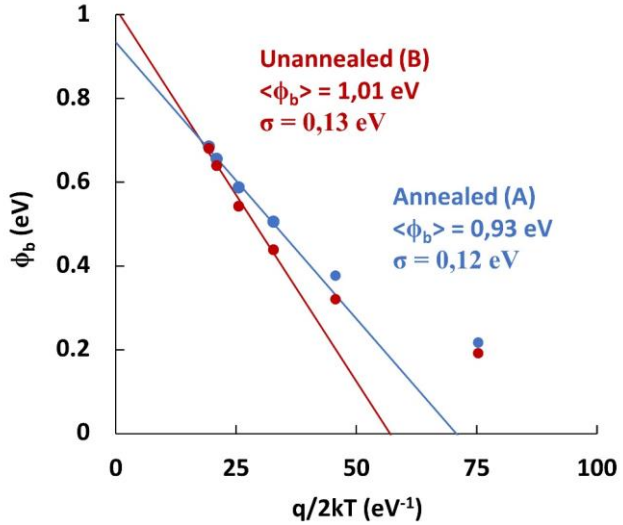

FIGURE 4. Schottky barrier height as a function of q/2kT. The solid lines fit are calculated from equation (3) (a).

rely on the dispersion of the barrier height, no more than the average height since device B suffer from more current leakage whereas it has approximately the same $<\phi_b>$ than sample A.

Because the previous model does not explain the improvement provided by the LTA, a second method studying the temperature dependence of the ideality factor η is investigated. In this model, others conduction modes than TE existing simultaneously are considered, such as the tunneling effect (TU) and the trap-assisted or field-enhanced TU mechanisms, and the field-enhanced thermionic emission (TFE). In this study, only the overall tunneling conduction is considered, hence the different tunneling conduction modes will be not distinguished. With regard to the measured Schottky barrier height in a Ni/AlGaN contact, the TE mode at room temperature cannot provide enough energy to the electron to cross the barrier, so TFE should be the main TE mode.

From η measurements, the tunneling parameter E_{00}, giving information about the TU contribution, can be extracted. *Figure 5a* shows a schematic representation of E_{00} on Ni/AlGaN/GaN band diagram. When $E_{00} >> kT$, the tunnel current is predominant on the overall current through the contact. When $E_{00} \sim kT$, the conduction is mainly ensured by the field-assisted thermionic emission[35]. In reverse bias, the tunnel current is added to the majority carrier saturation current specific to the TE mode, increasing the leakages. *Figure 5b* shows the ideality factor of each device as a function of temperature. At room temperature, η of 1.23 is measured on the annealed sample A, which shows good performance as compared to those found in literature[31,36,37], and 1.73 for sample B. Then, E_{00} is obtained using a regression of the η(T) curve according to the following Padovani equation[38]:

$$\eta(T) = \left(\frac{qE_{00}}{kT}\right) \cdot \coth\left(\frac{qE_{00}}{kT}\right), \qquad (4)$$

Where q, k and T are the elementary charge, the Boltzmann constant and the temperature respectively. Values of 27 meV and 38 meV are obtained for devices A and B respectively. In forward bias, the field enhanced thermionic emission is set as the main conduction mechanism in sample A when compared to the thermal energy kT/q at 300K (26 meV), while sample B suffers from more tunneling conduction. Nevertheless, it is a relatively good result when compared to other studies regarding Ni/AlGaN Schottky barrier

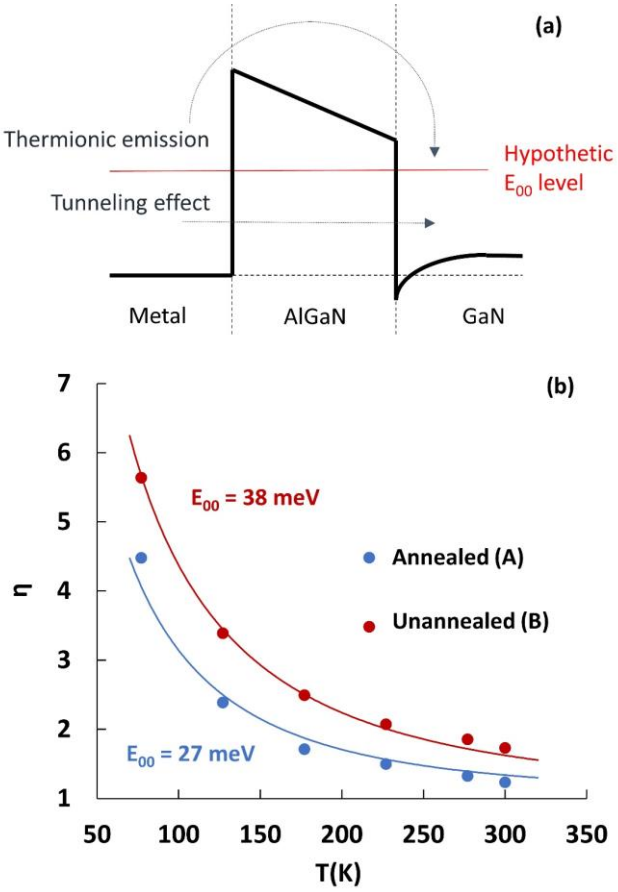

FIGURE 5. Schematic Ni/AlGaN/GaN band diagram indicating the preferred electron path according to the E_{00} level (a). Ideality factor as a function of temperature. Solid lines represent Padovani fits (b).

diodes. Lü et al.[39] obtained also a low E_{00} of 27 meV, but the literature reports a large range of values from few meV to 100 meV in most of cases[40–44].

To complete this analysis, the flat band barrier height ϕ_{FB} and the saturation current are calculated. Wagner et al.[45] formulated ϕ_{FB} by the following equation:

$$\phi_{FB} = \eta\phi_b - (\eta - 1) \cdot \frac{kT}{q} \cdot \ln\left(\frac{N_c}{N_D}\right), \quad (5)$$

$$\text{with } N_D = \varepsilon_{sc} m^* \cdot \left(\frac{2E_{00}}{\hbar}\right)^2, \quad (6)$$

Where N_c is the state density in the conduction band for $Al_{0.3}Ga_{0.7}N$, N_D is the AlGaN donor concentration, and ε_{sc}, m^* and $\hbar$ are the AlGaN permittivity, the electron effective mass and the reduced Planck constant, respectively. Donor concentrations of 2.10^{24} m^{-3} and $3.9.10^{24}$ m^{-3} are calculated for samples A and B respectively. Then, ϕ_{FB} of 0.88 eV for device A and 1.11 eV for device B are obtained, constituting approximatively the $<\phi_b>$ values found with the previous method. However, these results seems lower than those found in the literature. For example, Kim et al.[33], Lv et al.[46] and Greco et al.[47] found flat-band barrier heights of 1.4 eV, 1.6 eV and 1.12 eV, respectively, using the same method. Table 1 summarizes the results of both methods used. The saturation current I_S is

TABLE I. Comparison between Schottky barrier and theorical saturation current according both barrier calculation methods, and for samples A and B.

Method	Werner et al.		Wagner et al.	
Sample	$<\phi_b>$ (eV)	I_S (nA/mm)	ϕ_{FB} (eV)	I_S (nA/mm)
A	0.93	0.24	0.88	1.6
B	1.01	0.011	1.11	$2.3.10^{-4}$

given for each barrier values from (2). It appears that the TE reverse current contribution is always negligible compared to I_R, confirming that its reduction only depends on the tunneling effect lowering. However, the Ni/AlGaN contact still has to be improved before reaching its optimum behavior limit.

IV. SUMMARY AND CONCLUSIONS

In this paper, an improvement of reverse and forward characteristics of Ni/AlGaN on Si Schottky diodes, showing a low 0.54V on-voltage, is demonstrated using a long thermal annealing prior the Schottky contact deposition. The LTA permits a reduction of the contact serial on-resistance, divided by a factor two and thus enables higher current density than the non-annealed sample. Calculation shows first an equivalent barrier homogeneity of the Ni/AlGaN interface between both samples, and close barrier height values. Then, it appears that the LTA significantly reduces the ideality factor from 1.73 to 1.23. It permits a decrease of a decade regarding the tunneling reverse current, as it is still the main cause of leakage. These results open the door to low-losses and low-leakages GaN diodes for power electronics.

ACKNOWLEDGMENTS

This work was supported by the technology facility network RENATECH. This research work was partially undertaken with the support of IEMN fabrication (CMNF) and characterization (PCMP) platforms.

AUTHOR DECLARATIONS

Conflict of interest

The authors have no conflicts to disclose.

DATA AVAILABILITY

The data that support the findings of this study are available from the corresponding author upon reasonable request.

REFERENCES

[1]M. Xiao, Y. Ma, Z. Du, X. Yan, R. Zhang, K. Cheng, K. Liu, A. Xie, E. Beam, Y. Cao, H. Wang, and Y. Zhang, in 2020 IEEE International Electron Devices Meeting (IEDM) (2020), p. 5.4.1-5.4.4.

[2]S. L. Selvaraj, A. Watanabe, A. Wakejima, and T. Egawa, IEEE Electron Device Letters 33, 1375 (2012).

[3]Q. Zhou, Y. Jin, Y. Shi, J. Mou, X. Bao, B. Chen, and B. Zhang, IEEE Electron Device Lett. 36, 660 (2015).

[4]B. Li, Q. Li, F. C. Lee, Z. Liu, and Y. Yang, IEEE Journal of Emerging and Selected Topics in Power Electronics 6, 1627 (2018).

[5]L. Nela, R. Van Erp, G. Kampitsis, H. K. Yildirim, J. Ma, and E. Matioli, IEEE Transactions on Power Electronics 36, 1269 (2021).

[6]Q. Zhou, W. Xiong, X. Yang, L. Zhu, K. Chen, P. Huang, X. Ma, C. Zhou, W. Chen, and B. Zhang, IEEE Transactions on Electron Devices 67, 828 (2020).

[7]F. Zhou, W. Xu, Y. Jin, T. Zhou, F. Ren, D. Zhou, D. Chen, R. Zhang, Y. Zheng, and H. Lu, IEEE Transactions on Electron Devices 69, 5664 (2022).

[8]W. Jin Ha, S. Chhajed, S. Jae Oh, S. Hwang, J. Kyu Kim, J.-H. Lee, and K.-S. Kim, Appl. Phys. Lett. 100, 132104 (2012).

[9]K. Liu, C. Wang, X. Zheng, X. Ma, Y. Zhao, A. Li, Y. He, W. Mao, and Y. Hao, Phys. Status Solidi A 218, 2000686 (2021).

[10]Yong Cai, Yugang Zhou, K.J. Chen, and K.M. Lau, IEEE Electron Device Lett. 26, 435 (2005).

[11]Y.-H. Wang, Y.C. Liang, G.S. Samudra, P.-J. Chu, Y.-C. Liao, C.-F. Huang, W.-H. Kuo, and G.-Q. Lo, Semicond. Sci. Technol. 31, 025004 (2016).

[12]L. Efthymiou, G. Longobardi, G. Camuso, A.P.-S. Hsieh, and F. Udrea, in 2015 International Semiconductor Conference (CAS) (IEEE, Sinaia, Romania, 2015), pp. 211–214.

[13]T. Zhang, R. Li, Y. Zhang, H. Su, W. Zhang, X. Duan, J. Zhang, S. Xu, Y. Lv, and Y. Hao, Appl. Phys. Lett. 120, 232101 (2022).

[14]A. Li, C. Wang, Y. He, X. Zheng, X. Ma, Y. Zhao, K. Liu, and Y. Hao, Superlattices and Microstructures 156, 106952 (2021).

[15]E. Polyntsev, E. Erofeev, and I. Yunusov, Electronics 10, 2802 (2021).

[16]X. Kang, Y. Zheng, H. Wu, K. Wei, Y. Sun, G. Zhang, and X. Liu, Semiconductor Science and Technology 36, 094001 (2021).

[17]M.J. Wang, L. Yuan, K.J. Chen, F.J. Xu, and B. Shen, Journal of Applied Physics 105, 083519 (2009).

[18]K.J. Chen, L. Yuan, M.J. Wang, H. Chen, S. Huang, Q. Zhou, C. Zhou, B.K. Li, and J.N. Wang, in 2011 International Electron Devices Meeting (IEEE, Washington, DC, USA, 2011), p. 19.4.1-19.4.4.

[19]J.-C. Cheng and B.-Y. Tsui, IEEE Transactions on Electron Devices 65, 3739 (2018).

[20]C.F. Lo, T.S. Kang, L. Liu, C.Y. Chang, S.J. Pearton, I.I. Kravchenko, O. Laboutin, J.W. Johnson, and F. Ren, Appl. Phys. Lett. 97, 262116 (2010).

[21]J.H. Ye and M.S. Zhou, Journal of The Electrochemical Society 147, 1168 (2000).

[22]Z. Gao, B. Hou, Y. Liu, and X. Ma, Microelectronic Engineering 154, 22 (2016).

[23]J. Osvald, T. Lalinský, G. Vanko, Š. Haščík, and A. Vincze, Microelectronic Engineering 87, 2208 (2010).

[24]N.-H. Lee, M. Lee, W. Choi, D. Kim, N. Jeon, S. Choi, and K.-S. Seo, Jpn. J. Appl. Phys. 53, 04EF10 (2014).

[25]G. Kurt, M.E. Gulseren, G. Salkim, S. Ural, O.A. Kayal, M. Ozturk, B. Butun, M. Kabak, and E. Ozbay, IEEE J. Electron Devices Soc. 7, 351 (2019).

[26]B. Benakaprasad, A.M. Eblabla, X. Li, K.G. Crawford, and K. Elgaid, IEEE Transactions on Electron Devices 67, 863 (2020).

[27]H. Guan, G. Shen, B. Gao, H. Zhang, Y. Wang, and S. Wang, IEEE Access 9, 9855 (2021).

[28]Y. K. Yadav, B. B. Upadhyay, M. Meer, N. Bhardwaj, S. Ganguly, and D. Saha, IEEE Electron Device Letters 40, 67 (2019).

[29]H.-C. Chiu, J.-F. Chi, H.-L. Kao, C.-Y. Chu, K.-L. Cho, and F.-T. Chien, Microelectronics Reliability 59, 44 (2016).

[30]J.H. Werner and H.H. Güttler, Journal of Applied Physics 69, 1522 (1991).

[31]J.-H. Shin, J. Park, S. Jang, T. Jang, and K. Sang Kim, Appl. Phys. Lett. 102, 243505 (2013).

[32]S. Karboyan, J.G. Tartarin, and B. Lambert, Analysis of Barrier Inhomogeneities in AlGaN/GaN HEMTs' Schottky Diodes by I-V-T Measurements (2013), p. 243.

[33]H. Kim, S. Choi, and B.J. Choi, Coatings 10, 194 (2020).

[34]M. Garg, A. Kumar, H. Sun, C.-H. Liao, X. Li, and R. Singh, Journal of Alloys and Compounds 806, 852 (2019).

[35]I. Jabbari, M. Baira, H. Maaref, and R. Mghaieth, Chinese Journal of Physics 73, 719 (2021).

[36]S. Saadaoui, M. Mongi Ben Salem, M. Gassoumi, H. Maaref, and C. Gaquière, Journal of Applied Physics 110, 013701 (2011).

[37]G. Greco, P. Fiorenza, M. Spera, F. Giannazzo, and F. Roccaforte, Journal of Applied Physics 129, 234501 (2021).

[38]F.A. Padovani and R. Stratton, Solid-State Electronics 9, 695 (1966).

[39]Y.-J. Lü, Z.-H. Feng, Z.-J. Lin, G.-D. Gu, S.-B. Dun, J.-Y. Yin, T.-T. Han, and S.-J. Cai, Chinese Physics B 23, 027101 (2014).

[40]D. Yan, J. Jiao, J. Ren, G. Yang, and X. Gu, Journal of Applied Physics 114, 144511 (2013).

[41]E. Arslan, Ş. Altındal, S. Özçelik, and E. Ozbay, Semiconductor Science and Technology 24, 075003 (2009).

[42]M. Siva Pratap Reddy, A. Bengi, V. Rajagopal Reddy, and J.-S. Jang, Superlattices and Microstructures 86, 157 (2015).

[43]A.R. Arehart, B. Moran, J.S. Speck, U.K. Mishra, S.P. DenBaars, and S.A. Ringel, Journal of Applied Physics 100, 023709 (2006).

[44]R.P. Tompkins, M.R. Khan, R. Green, K.A. Jones, and J.H. Leach, J Mater Sci: Mater Electron 27, 6108 (2016).

[45]L.F. Wagner, R.W. Young, and A. Sugerman, IEEE Electron Device Lett. 4, 320 (1983).

[46]Y. Lv, Z. Lin, T.D. Corrigan, J. Zhao, Z. Cao, L. Meng, C. Luan, Z. Wang, and H. Chen, Journal of Applied Physics 109, 074512 (2011).

[47]G. Greco, F. Giannazzo, and F. Roccaforte, Journal of Applied Physics 121, 045701 (2017).